Ceramics International 51 (2025) 24574–24582

Contents lists available at ScienceDirect

Ceramics International

journal homepage: www.elsevier.com/locate/ceramint

The effects of co-implanting strontium (Sr) and helium (He) into SiC at temperatures exceeding the critical amorphization temperature and annealing above 1000 °C

T.T. Hlatshwayo [a,*], T.F. Mokgadi [a], S.S. Ntshangase [b], Z.A.Y. Abdalla [a], E.G. Njoroge [a,c], T. Nguyen [d], A. Sohatsky [d], V.A. Skuratov [d,e,f]

[a] Physics Department, University of Pretoria, Private Bag X20, 0028, Hatfield, South Africa
[b] Department of Physics, University of Zululand, P/B X1001, KwaDlangezwa, 3886, South Africa
[c] ENGAGE, University of Pretoria, Private Bag X20, 0028, Hatfield, South Africa
[d] Joint Institute for Nuclear Research, Dubna, Russia
[e] National Research Nuclear University MEPhI, Moscow, Russia
[f] Dubna State University, Dubna, Moscow region, Russia

ARTICLE INFO

Handling Editor: Dr P. Vincenzini

Keywords:
RBS
Helium
Blisters
Helium-induced voids
Helium-induced cavities
Sr migration

ABSTRACT

The structural evolution and migration behaviour of strontium (Sr) in polycrystalline silicon carbide (SiC) co-implanted with helium (He) exceeding 300 °C were investigated at temperatures above 1000 °C. Sr ions were implanted into SiC at 600 °C (denoted as Sr-SiC-600) and co-implanted with He ions at 350 °C (denoted as Sr + He-SiC-600). Both samples were subsequently isochronally annealed at 1100 °C, 1200 °C, and 1300 °C for 5 h. Both as-implanted and annealed were characterized by transmission electron microscopy (TEM), scanning electron microscopy (SEM), atomic force microscopy (AFM), and Rutherford backscattering spectrometry (RBS). Implantation at 600 °C resulted in a defective layer embedded in the crystalline SiC. Co-implantation led to the formation of He platelets in the defective layer, as well as blisters and large voids on the surface accompanied by slight migration of Sr. Annealing the Sr-SiC-600 samples up to 1300 °C resulted in formation of Sr precipitates accompanied by neither migration nor loss. Contrary annealing Sr + He-SiC-600 samples up to 1300 °C resulted in the formation of Sr precipitates accompanied by some loss of Sr. These results indicate trapping of Sr in both samples. This trapping was influenced by thermally activated cavities in the Sr-SiC-600 samples and by He induced cavities in the Sr + He-SiC-600 samples. These findings have significant implications for the design and performance of TRISO fuel particles.

1. Introduction

Silicon carbide (SiC) is widely used in various harsh environments, including modern fission nuclear reactors, due to its exceptional physical and chemical properties. These include high hardness, wear resistance, low density, high strength, oxidation resistance, chemical resistance, excellent high-temperature stability, low thermal expansion, high thermal conductivity, excellent thermal shock resistance, low neutron activation, and a low neutron absorption cross-section [1,2]. In modern nuclear reactors, chemical vapor deposited (CVD) 3C-SiC (SiC) serves as the primary diffusion barrier for fission products (FPs) within coated tri-structural isotropic (TRISO) fuel particles. This enhances the retention of radioactive fission products, thereby improving reactor safety [3]. Under normal operation within the temperature range of 900–1300 °C, TRISO fuel particles retain most radiologically significant fission products, with notable exceptions such as strontium (Sr), cesium (Cs), and silver (Ag) [4,5].

During fission, a high flux of energetic neutrons is produced. Some of these neutrons interact with the SiC crystal structure through inelastic and elastic collisions, creating vacancies, interstitials, and other defects. Others are captured by target nuclei, resulting in nuclear transmutations and the formation of impurities such as helium (He) [6–9]. At the elevated operating temperatures in modern fission nuclear reactors, phenomena such as gas release, defect coalescence, and the accumulation of mobile defects contribute to the formation of larger structural imperfections, including He bubbles and cavities [10,11]. He ions

* Corresponding author.
E-mail address: thulani.hlatshwayo@up.ac.za (T.T. Hlatshwayo).

https://doi.org/10.1016/j.ceramint.2025.03.140
Received 4 October 2024; Received in revised form 15 January 2025; Accepted 10 March 2025
Available online 10 March 2025
0272-8842/© 2025 The Authors. Published by Elsevier Ltd. This is an open access article under the CC BY license (http://creativecommons.org/licenses/by/4.0/).

precipitate to form bubbles or platelets under high internal pressure, which can grow and manifest as blisters on the surface [12,13]. Prolonged irradiation at elevated temperatures may cause these blisters to rupture, releasing gas atoms and fragmenting the host material [14]. Therefore, to fully understand the release of fission products (FPs) in modern fission reactors, it is essential to investigate their behaviour in the presence of He at elevated temperatures.

To the best of our knowledge, several studies have investigated the structural evolution of SiC pre-implanted with heavy ions (such as krypton (Kr), iron (Fe), and strontium (Sr)) and helium at room temperature (RT) [15–22]. However, limited research has been conducted under similar conditions at elevated temperatures [23–25]. The co-implantation of He into SiC pre-implanted with heavy ions at RT leads to the formation of nano-sized He bubbles within the amorphous SiC layer [15–22]. Annealing these samples at temperatures ranging from 1000 °C to 1300 °C results in the formation of He bubbles, blisters, and craters (He-induced voids) [21,22]. Additionally, He cavities have been shown to trap implanted Sr, although some Sr loss occurs through holes in the co-implanted samples annealed up to 1300 °C [21,22]. In contrast, co-implantation at temperatures above 300 °C leads to the formation of He bubbles, platelets, blisters, and craters [23–25]. Annealing at 1000 °C and 1100 °C causes the He bubbles to grow larger by capturing additional vacancies, which facilitates the migration of Sr toward the bulk and surface, accompanied by some loss through holes [23–25].

Given that modern fission reactors operate at elevated temperatures, it is crucial to understand the impact of He on SiC's structure and how it influences the migration of key fission products, such as Sr, during implantation and subsequent annealing. However, this area remains largely unexplored, particularly at annealing temperatures above 1000 °C for SiC that has been pre-implanted and co-implanted at temperatures exceeding the critical amorphization temperature of SiC.

To address this knowledge gap, we conducted a comprehensive investigation into the structural evolution of SiC and the migration behaviour of Sr in SiC co-implanted with Sr and He at temperatures exceeding 300 °C, followed by annealing at temperatures above 1000 °C. In this study, Sr ions were initially implanted into SiC at 600 °C, with some samples subsequently co-implanted with He ions at 350 °C. Both individually implanted and co-implanted samples were then annealed at temperatures above 1000 °C. The as-implanted and annealed samples were characterized using TEM, SEM, AFM and RBS. The results from the individually implanted and co-implanted SiC samples were compared to investigate the roles of He and annealing.

2. Experimental methods

Polycrystalline SiC from Valley Design Corporation, primarily composed of 3C-SiC with trace amounts of 6H-SiC [26], was used as the starting material for this study. Sr ions were implanted into the SiC at 600 °C with an energy of 360 keV to a fluence of 2×10^{16} cm^{-2} (referred to as Sr-SiC-600). Some of the Sr-SiC-600 samples were further co-implanted with He ions at 21.5 keV at 350 °C to a fluence of 1×10^{17} cm^{-2} (referred to as Sr + He-SiC-600). Detailed experimental procedures for both Sr and He ion implantation can be found in Refs. [21–23].

The as-implanted Sr-SiC-600 and Sr + He-SiC-600 samples were isochronally annealed in vacuum (10^{-5} Pa) for 5 h at temperatures of 1100 °C, 1200 °C, and 1300 °C. Characterization of the samples was performed both before and after annealing using transmission electron microscopy (TEM), scanning electron microscopy (SEM), and Rutherford backscattering spectrometry (RBS). Additionally, atomic force microscopy (AFM) was used to characterize the as-implanted and annealed Sr + He-SiC-600 samples.

TEM lamellae of the as-implanted and annealed samples were prepared using a FEI Helios Nanolab 650 focused ion beam (FIB), with detailed lamella preparation procedures outlined in Refs. [21–23]. For characterization, scanning TEM (STEM) equipped with high-angle annular dark field (HAADF) and energy-dispersive X-ray spectroscopy (EDS) detectors was used to investigate the distribution of Sr atoms. TEM analysis was performed using a Thermo Scientific Talos F200i field emission transmission electron microscope, operating at an acceleration voltage of 200 kV. SEM imaging of the surfaces of the Sr-SiC-600 and Sr + He-SiC-600 samples, both before and after annealing, was conducted using a Zeiss Gemini Ultra Plus field emission gun scanning electron microscope (FEG-SEM). Imaging was performed with an in-lens detector and an accelerating voltage of 2 kV. The Sr + He-SiC-600 samples, before and after annealing, were also characterized using a Bruker Dimension Icon with ScanAsyst AFM system in contact mode. AFM micrographs were analyzed using NanoScope Analysis software. Rutherford backscattering spectrometry (RBS) measurements were carried out at room temperature (RT) using a 2.0 MeV He^{+} beam with a current of approximately 500 pA, and a total charge of 0.5 μC per measurement. Backscattered particles were detected using a solid-state detector at a backscattering angle of 150°. The RBS spectra were converted into depth profiles using energy loss data provided by Ziegler [27] and a SiC density of 3.21 g/cm^3.

3. Results

Fig. 1 shows dark field (DF) STEM and high-angle annular dark field (HAADF) STEM micrographs of the as-implanted Sr-SiC-600 sample, as well as those of the Sr-SiC-600 samples annealed at 1100 °C and 1300 °C. Selected area diffraction (SAD) patterns of the defective regions are also shown in Fig. 1. Sr implantation resulted in the formation of an implanted layer consisting of a less defective SiC region extending from the surface to approximately 96 nm, and a highly defective or strained region extending from 96 nm to around 296 nm below the surface (indicated by the dotted lines in Fig. 1(a)). The width of the highly defective layer, compared to the projected range of 360 keV Sr ions in SiC (approximately 140 nm, as reported in Refs. [21–23]), along with the relatively brighter region observed in the HAADF STEM micrograph (Fig. 1(d)) and the Sr EDS map (Fig. S1), suggests that most of the implanted Sr is incorporated within the highly defective or strained region. In the HAADF STEM micrograph, the contrast observed is related to the atomic number (Z) of the elements in the sample. Regions with higher contrast or brightness correspond to elements with higher atomic numbers (Z), while darker regions indicate elements with lower Z. The DF-STEM micrograph of the as-implanted samples reveals varying brightness within the highly defective layer, suggesting the presence of crystallites and defects. Additionally, the SAD pattern from this highly defective layer exhibits a mix of circular and elongated diffraction spots, which indicates the presence of crystalline SiC with defects. The absence of amorphization was expected, as the implantation temperature exceeded the critical amorphization threshold of approximately 300 °C [28]. This observation is in line with previous studies on the implantation of 360 keV Sr ions into SiC at 600 °C [29,30].

Annealing the Sr-SiC-600 samples at 1100 °C and 1300 °C for 5 h led to the recrystallization of the defective layer, with more pronounced recrystallization observed at higher annealing temperatures. This is reflected in the increased brightness of the defective layers (Fig. 1(b) and (c)) and the corresponding diffraction patterns (Fig. 1(h) and (i)). At 1100 °C, annealing induced a noticeable increase in brightness in the middle of the highly defective layer, although no significant changes were observed in the HAADF STEM micrograph, indicating the absence of Sr precipitates (Fig. 1(e) and (f)). In contrast, annealing at 1300 °C led to the formation of a high density of nanometer-sized metal precipitates, concentrated in the middle of the highly defective layer (Fig. 1(f) and Fig. S1). The crystalline nature of these Sr precipitates was confirmed by their SAD patterns (Fig. 1(i)). Furthermore, Sr EDS depth profiles and maps of both the as-implanted and annealed layers revealed high-contrast spots corresponding to Sr precipitates, located near the projected range (see Fig. S1 in the supplementary data).

Fig. 2 shows the under-focused (uf.) bright-field (BF) TEM, DF-STEM,

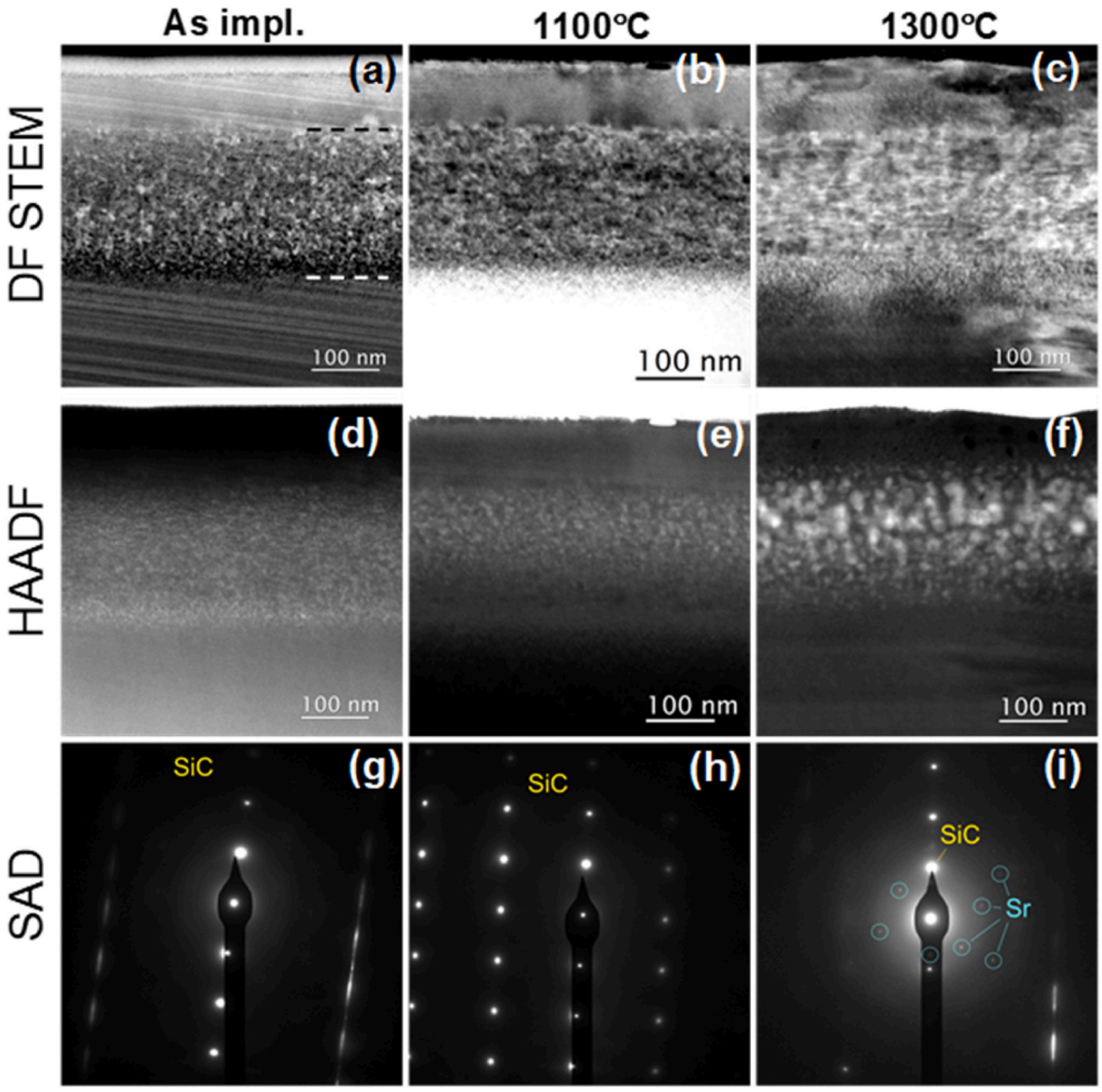

Fig. 1. DF-STEM micrographs of as-implanted Sr-SiC-600 (a) and Sr-SiC-600 annealed at 1100 °C (b) and 1300 °C (c) respectively, HAADF-STEM micrographs of as-implanted Sr-SiC-600 (d) and Sr-SiC-600 annealed at 1100 °C (e) and 1300 °C (f), respectively. The selected area diffraction patterns of their highly defective regions are also shown in (g), (h) and (i).

and HAADF micrographs of the as-implanted and annealed Sr + He-SiC-600 samples. Co-implantation with He resulted in the formation of He nano-bubbles and elongated platelets, which were aligned parallel to the surface within the highly defective region (Fig. 2(a)). It is well-established that He implantation at temperatures below the critical amorphization temperature of SiC induces the formation of nano-bubbles. However, when He is implanted at temperatures above this threshold, both He nano-bubbles and platelet formation are observed in SiC [7,9,10,16–23,30–42]. This behaviour is expected, as the higher defect density in amorphous SiC provides more nucleation sites, thereby promoting the formation of He bubbles compared to SiC with fewer defects [42].

When He ions are implanted into SiC, they do not directly bond with the carbon or silicon atoms but rather interact with the lattice in a way that generates vacancies and other point defects. This occurs because He is a noble gas and does not readily form strong bonds with the Si or C atoms. The implanted He atoms accumulate in the lattice and form vacancy-He complexes or interstitial- He complexes. These defects, particularly He-vacancy clusters, can create localized distortions in the lattice, leading to changes in the overall material structure. As the concentration of He increases, He atoms tend to cluster together due to their low atomic size and may accumulate in interstitial sites or vacancy clusters to form He bubbles. This can lead to local swelling and pressure build up in the material, causing mechanical stress that may affect the migration of FPs in SiC. The formation of He platelets in Sr + He-SiC-600 is attributed to the defects created by Sr implantation, which act as additional nucleation sites, facilitating the formation of He platelets. The complex interactions between Sr, He, and the SiC lattice lead to a unique structural evolution, which is not typically observed when He is implanted alone [11].

The He-induced defects can significantly impact the structural integrity of the substrate, potentially leading to surface swelling, crack formation, and surface exfoliation. Similar to the DF-STEM micrograph of the as-implanted Sr-SiC-600, the DF-STEM micrograph of the highly defective Sr + He-SiC-600 layer reveals areas of varying brightness, indicating crystallites and defects (Fig. 2(d)). This observation supports the absence of amorphization, as confirmed by the SAD patterns (Fig. 2 (j)). Additionally, the HAADF micrograph shows a uniform distribution

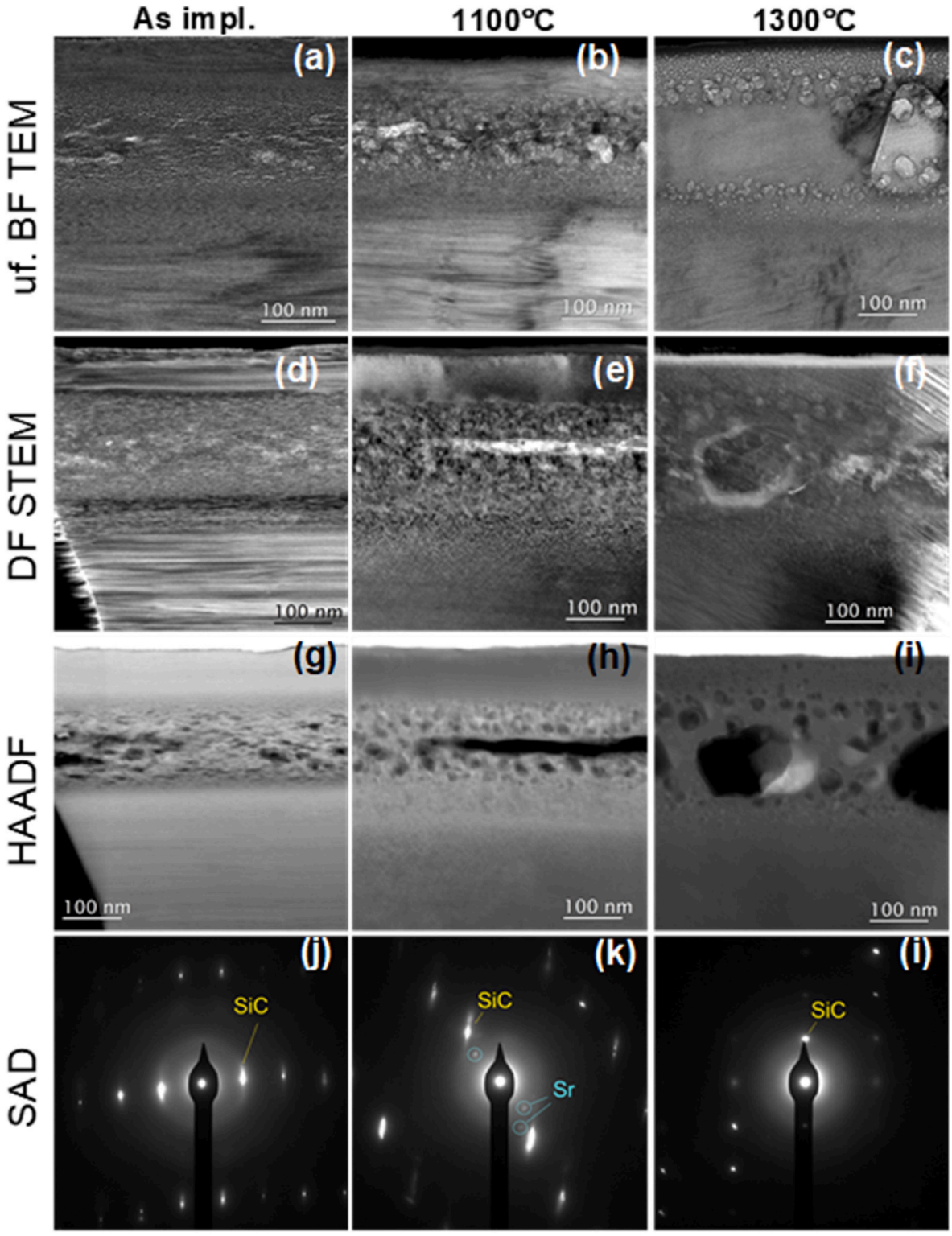

Fig. 2. Under focus bright field (BF) TEM micrographs of as-implanted Sr + He-SiC-600 (a) and Sr + He-SiC-600 annealed at 1100 (b) and 1300 °C (c) respectively, DF STEM micrographs of as-implanted Sr + He-SiC-600 (d) and Sr + He-SiC-600 annealed at 1100 (e) and 1300 °C (f), HAADF-STEM micrographs of as-implanted Sr + He-SiC-600 (g) and Sr + He-SiC-600 annealed at 1100 (h) and 1300 °C (i). The selected area diffraction patterns of their defective regions are also shown in (j), (k) and (l).

of implanted Sr (Fig. 2(g)), which is further corroborated by the Sr EDS maps and depth profiles (Fig. S2).

Annealing the Sr + He-SiC-600 samples at 1100 °C and 1300 °C led to an increase in the size of helium bubbles, the formation of He-induced cavities, and the elongation and widening of the He platelets (Fig. 2(b) and (c)). While the size of the bubbles increased in the sample annealed at 1100 °C, it decreased in the sample annealed at 1300 °C. This trend occurs because the concentration of He decreases with higher annealing temperatures due to the diffusion of He out of the voids created on the sample surface (further details on voids and blisters can be found in the

AFM results). In the 1300 °C annealed sample (Fig. 2(c)), two distinct bubble layers are observed: one closer to the surface and another near the end-of-range of the highly defective layer.

Helium tends to accumulate in regions with pre-existing defects. When the concentration of He atoms exceeds the solubility limit of He in the SiC lattice, bubble formation occurs. These He bubbles are essentially cavities filled with He atoms. As the He gas expands, the cavities also grow, and when the gas escapes, empty spaces or cavities are left behind. The separation of the bubble layer in the 1300 °C annealed sample is attributed to the formation of larger cavities at the center of the defective layer, which causes the redistribution of defects toward the periphery. Additionally, Sr precipitates were observed in the Sr + He-SiC-600 samples annealed at both 1100 °C and 1300 °C (Fig. 2(h), (i), and Fig. S2). In the samples annealed at 1100 °C, these precipitates are polycrystalline (Fig. 2(k)), while in the samples annealed at 1300 °C, they are trapped within the He-induced cavities (Fig. 2(i) and Fig. S2).

The surface morphological changes before and after annealing were observed using SEM. Fig. 3 presents the SEM micrographs of both the as-implanted and annealed Sr-SiC-600 and Sr + He-SiC-600 samples. The surface of the as-implanted Sr-SiC-600 sample (Fig. 3(a)) shows scratch marks, which are commonly observed in pristine SiC [43]. These scratch marks are a result of the mechanical polishing process carried out by the manufacturer. This observation indicates the absence of amorphization in the as-implanted Sr-SiC-600 sample. Implantation of SiC with heavy ions at room temperature and high fluence typically leads to substrate amorphization, which is characterized by a featureless structure [2]. In contrast, when SiC is implanted with heavy ions above the critical amorphization temperature, the substrate remains crystalline with minimal point defects [28,44], often exhibiting scratch marks and, in some cases, visible grains or crystals. The crystallinity and minimal defects observed in the as-implanted Sr-SiC-600 sample are consistent with the TEM results discussed earlier. Additionally, the surface of the as-implanted Sr-SiC-600 sample is relatively smooth and even, with some grain boundaries visible. No significant changes were observed in the Sr-SiC-600 sample annealed at 1100 °C (Fig. 3(b)), suggesting that surface recrystallization depends on the underlying crystalline region rather than the defective region. This is further supported by bright-field TEM images, which reveal a sufficiently large crystalline layer beneath the surface before encountering the defective region. In the Sr-SiC-600 samples annealed at 1200 °C and 1300 °C (Fig. 3(c) and (d)), small voids or holes appear at the grain boundaries. These voids are more pronounced in the 1200 °C compared to the 1300 °C annealed samples. The difference might be due to higher recrystallization rate at 1300 °C. These openings result from thermal etching during the annealing process, which preferentially affects the grain boundaries [45].

Co-implantation of He led to the appearance of irregular surface structures that were not present in the as-implanted Sr-SiC-600 samples, indicating that these structures were induced by He implantation. Additionally, polishing marks were less visible in the as-implanted Sr + He-SiC-600 micrographs, which can be attributed to surface swelling caused by the formation of helium bubbles and platelets beneath the surface. Similar observations have been reported in previous studies [39]. Annealing the Sr + He-SiC-600 sample at 1100 °C resulted in the reappearance of polishing marks, along with the emergence of crystals and grain boundaries. Despite this, irregular structures caused by He-induced defects were still visible, suggesting that surface recrystallization occurred, but some He-induced defects remained. In the Sr + He-SiC-600 samples annealed at 1200 °C and 1300 °C (Fig. 3(c') and (d')), small voids or cracks appeared due to thermal etching, similar to the Sr-SiC-600 samples annealed at these temperatures. However, irregular helium-induced structures remained present.

To investigate the nature of the irregular structures in the Sr + He-SiC-600 samples, additional analysis was performed using AFM. Fig. 4 presents the AFM micrographs of the Sr + He-SiC-600 samples before and after annealing. The AFM micrograph of the as-implanted Sr + He-SiC-600 sample reveals darker and brighter areas, corresponding to He-induced voids and He-filled blisters, respectively. Consistent with TEM results, He implantation at 350 °C leads to the formation of bubbles and platelets beneath the surface, which subsequently cause surface swelling. The He-filled blisters observed in the as-implanted sample are a result of bubble growth beneath the surface during implantation. The exfoliated blisters, or He-induced voids, are caused either by the eruption of bubbles due to He-ion sputtering during implantation or by the eruption of unstable, highly pressurized blisters [41,45,46]. Voids form as He gas is released and SiC fragments, while blisters appear on the surface as the underlying bubbles expand. These expanding bubbles form a connected network parallel to the surface, causing radial swelling and the eventual appearance of blisters. When the blisters exfoliate, they leave behind large voids, potentially causing the loss of implanted ions in the surrounding regions. In alignment with the SEM micrographs, the as-implanted sample shows no polishing marks, confirming surface swelling due to He bubbles. Annealing the Sr + He-SiC-600 samples at 1100 °C resulted in the appearance of larger helium-induced voids and a reduced density of blisters, along with the re-emergence of polishing marks, indicating surface recrystallization. However, the samples annealed at 1200 °C and 1300 °C showed no polishing marks, which can be attributed to the increased size of bubbles and cavities beneath the surface. These higher annealing temperatures led to the formation of

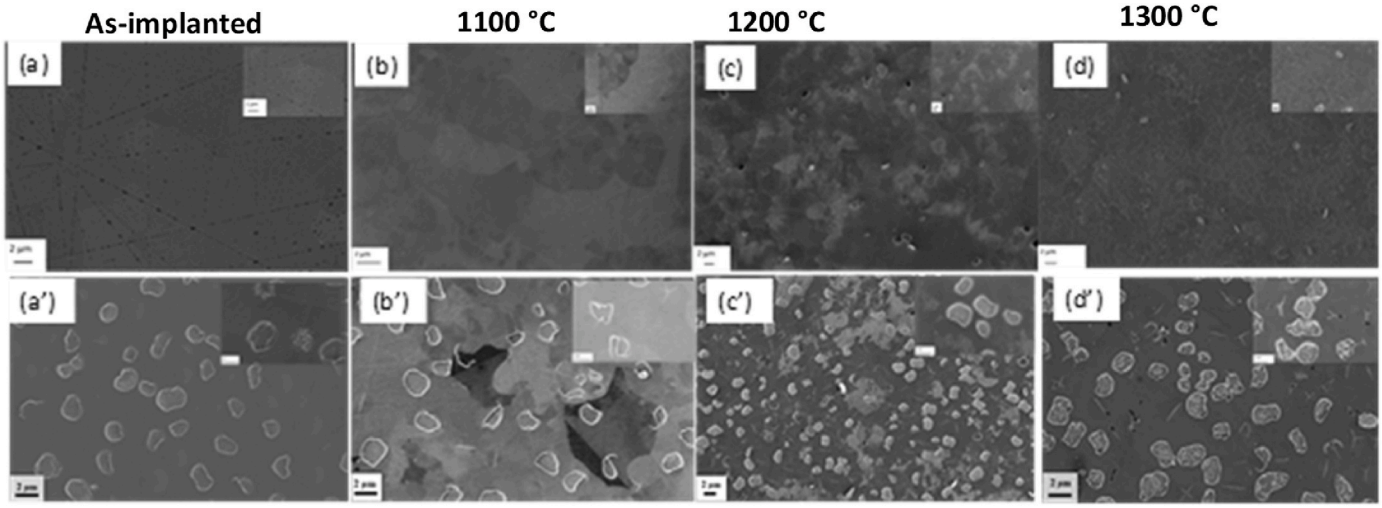

Fig. 3. Surface SEM micrographs of (a) as-implanted Sr-SiC-600 and (a') as-implanted Sr + He-SiC-600 samples, (b–d) isochronally annealed Sr-SiC-600 samples, and (b'-d') isochronally annealed Sr + He-SiC-600 samples. The samples were isochronally annealed at 1100 °C; 1200 °C, and 1300 °C for 5 h, respectively.

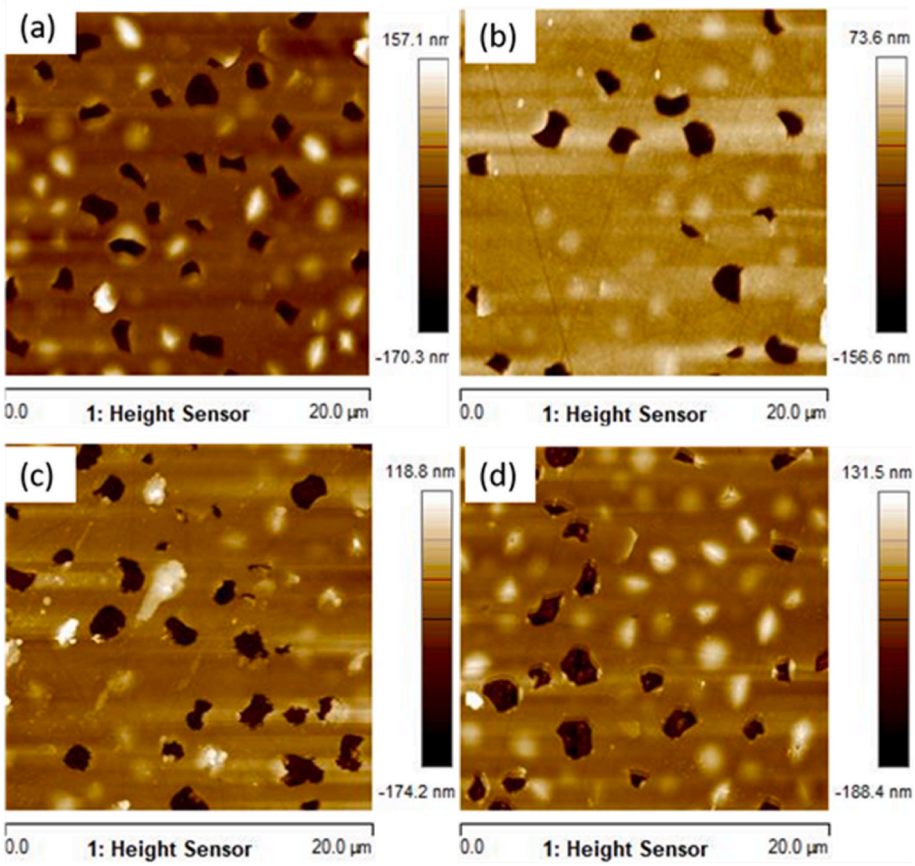

Fig. 4. AFM micrographs of as-implanted Sr + He-SiC-600 (a), and Sr + He-SiC-600 annealed at (b) 1100 °C; (c) 1200 °C; and (d) 1300 °C for 5 h.

even larger voids and blisters, with the sample annealed at 1300 °C exhibiting particularly pronounced blisters, indicating significant growth of helium bubbles beneath the surface.

The migration of implanted Sr was monitored before and after annealing using Rutherford Backscattering Spectrometry (RBS). Fig. 5 presents the Sr depth profiles for the Sr-SiC-600 and Sr + He-SiC-600 samples, before and after annealing. Fig. 5 also includes the corresponding Sr retention ratios and full width at half maximum (FWHM) as a function of annealing temperature. Approximately 13 % of Sr was lost in the samples annealed at 1200 °C. This loss at 1200 °C may be due to the lack of cavities in the defective SiC, which restricts Sr migration at this temperature, as well as the appearance of more pores on the surface (More pores at 1200 °C, which enhances Sr migration (Fig. 3(c) compared to (d)). No cavities were observed in the TEM images of the 1100 °C annealed samples. Additionally, changes in the shape of the Sr depth profile for the 1300 °C annealed samples, likely caused by the formation of Sr precipitates (as shown in Fig. 1 and Fig. S1), were reflected in slight alterations to the RBS profiles. These observations contrast with those reported by Friedland et al. [29], who studied CVD polycrystalline SiC, where 360 keV Sr ions were implanted at 600 °C followed by sequential annealing at temperatures ranging from 1000 to 1400 °C. In their study, minimal Sr migration was observed up to 1200 °C, with significant broadening occurring only at 1300 °C and above. The discrepancies between their findings and the present study may be attributed to differences in the annealing methods: sequential annealing in Ref. [29] versus isochronal annealing in the current work. In sequential annealing, the sample undergoes a series of temperature steps, while isochronal annealing involves individual samples being annealed at each temperature. In sequential annealing, changes to the surface or structure at lower temperatures may influence the behaviour at higher temperatures, potentially explaining the differences in Sr migration observed in their study.

Fig. 5(c) and (d) show the Sr depth profiles of the Sr + He-SiC-600 samples before and after annealing, along with their FWHM and retained Sr ratios as a function of annealing temperature. The loss of Sr in the as-implanted Sr + He-SiC-600 samples can be attributed to the formation of bubbles and voids during He co-implantation. Annealing the Sr + He-SiC-600 samples at 1100 °C resulted in an approximately 18 % loss of implanted Sr, with no broadening observed in the FWHM. As the annealing temperature increased to 1300 °C, the loss of Sr continued, accompanied by broadening of the FWHM at temperatures above 1100 °C. The loss of implanted Sr, without any significant peak shifts in the annealed Sr + He-SiC-600 samples, suggests that Sr is trapped in the defective regions (as seen in Fig. 2 and S2). The observed peak broadening, particularly in the 1300 °C annealed sample, is linked to the surface roughness observed in the AFM results (Fig. 4). Thus, helium-induced cavities can trap Sr, while the formation of pores contributes to the loss of Sr.

Previous studies have demonstrated similar agglomeration behaviour of implanted species in SiC for various elemental implants [2]. Specifically, when SiC is implanted at elevated temperatures and subsequently annealed in the range of 1250–1500 °C, cavities form within the material. Elements such as Ag, I, Cs, and Sr tend to occupy these cavities and form nanocrystals [2]. The formation of bubbles is known to impede the migration of defects, such as Frenkel pairs, dislocation loops, and stacking faults [47–51], resulting in increased stress and strain in the defective layer after annealing. This process can lead to in crack and cavity formation, especially at the center of the defective region. Consequently, Sr atoms tend to agglomerate and occupy these cavities, leading to the formation of Sr nanocrystals. This is supported by the Sr EDX distributions and HAADF-STEM results shown in Fig. 2 and S2.

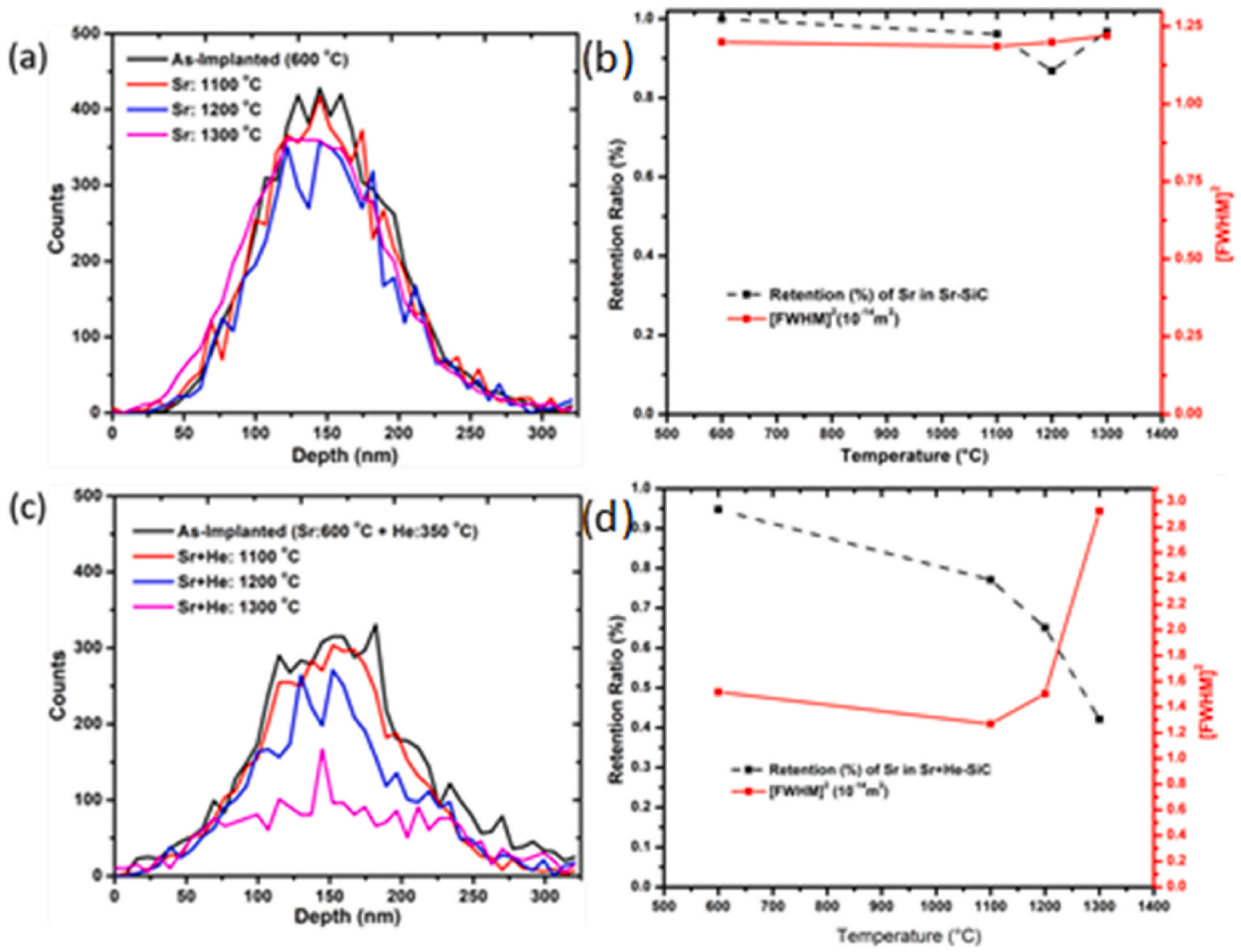

Fig. 5. (a) Depth profile of Sr in Sr-SiC-600 before and after annealing at temperatures ranging from 1100 °C to 1300 °C for 5 h. (b) Full-width at half maximum (FWHM) and retention ratio of Sr in Sr-SiC-600. (c) Depth profile of Sr in Sr + He-SiC-600 before and after vacuum annealing at temperatures ranging from 1100 °C to 1300 °C for 5 h. (d) FWHM and retention ratio of Sr in Sr + He-SiC-600.

4. Discussion

The migration of Sr in Sr-SiC-600 samples annealed at temperatures above 1000 °C, up to 1300 °C, is minimal. This can be attributed to a trapping mechanism, where Sr atoms migrate into cavities that form within the defective SiC at high annealing temperatures, ultimately leading to the formation of precipitates. These observations are confirmed by TEM, STEM, and EDS analyses, with additional support from RBS results.

The implantation of He into Sr pre-implanted SiC led to the migration of some Sr atoms into the substrate and toward the surface. Additionally, there was a loss of approximately 5 % of the initial Sr concentration in the as-implanted Sr + He-SiC-600 compared to the as-implanted Sr-SiC-600. This loss can be attributed to the high temperature during the He implantation process. The migration and loss of Sr were caused by the following factors: (1) Bubble formation – During implantation, bubbles form at the regions with the highest concentration of defects below the surface. These bubbles cause swelling in the defective region, leading to the migration of Sr atoms from their original location. (2) Helium-induced void formation – The high temperatures during implantation promote the growth of bubbles, which eventually form blisters on the surface. When these blisters reach a critical size in terms of diameter and height, they exfoliate. The critical pressure exerted by He on the blister walls, combined with a stress intensity factor at the crack tip exceeding the material's fracture toughness [41], results in the formation voids extending into the defective region. These voids facilitate the migration and out-diffusion of Sr atoms.

Thermal annealing of the Sr-SiC-600 samples resulted in the formation of cavities at temperatures above 1100 °C. In contrast, the Sr + He-SiC-600 samples exhibited the formation of He-induced cavities starting at 1100 °C. These cavities, caused by He out-diffusion, served as sites for the entrapment of Sr nanocrystals. With increasing temperature, the cavities expanded, accommodating more Sr atoms within them.

However, a significant difference arises in Sr loss. While Sr nanocrystals are trapped within the growing cavities, the presence of exfoliated blisters extending as deep as the projected range of Sr results in a faster rate of Sr loss in the Sr + He-SiC-600 samples compared to their Sr-SiC-600 counterparts. This distinctive behaviour underscores the complex interplay of processes governing Sr migration and retention in these materials.

It is important to note that Sr trapping occurs in both Sr-SiC-600 and Sr + He-SiC-600 samples. In the Sr-SiC-600 samples, trapping is driven by high-temperature annealing, whereas in the Sr + He-SiC-600 samples, it results from a combination of high-temperature annealing and the presence of He contributes to Sr. Although the results of this study are specific to the SiC used, which closely resembles the material used in

modern nuclear reactors, further investigations involving different SiC polytypes will be conducted to assess whether these findings can be generalized to other forms of SiC.

5. Conclusion

This study investigated the structural changes and migration behaviour of Sr in SiC co-implanted with Sr and He ions. The experimental procedure involved implanting 360 keV Sr ions into SiC at an elevated temperature of 600 °C. Some samples were later implanted with 21.5 keV He ions at 350 °C. The single and co-implanted SiC samples were subsequently annealed at 1100 °C, 1200 °C, and 1300 °C for 5 h. The high-temperature implantation process preserved the crystalline structure of SiC with minimal defects. During annealing, the defective regions in the Sr-SiC-600 samples developed a consistent surface pattern with a preferred orientation. Annealing at 1200 °C led to the formation of voids within the grain boundaries. Overall, the annealing of Sr-SiC-600 samples resulted in negligible Sr migration. However, Sr precipitates were observed at 1300 °C attributed to the formation of thermally-induced cavities that trapped Sr nanocrystals.

The Sr + He-SiC-600 samples also exhibited surface recrystallization, along with the formation of small thermally-etched voids, larger He-induced voids, and He-filled blisters. Annealing at 1100 °C led to the formation of small He-induced cavities that trapped Sr atoms. As the annealing temperature increased, these cavities expanded, accommodating more Sr atoms. The co-implantation of He with Sr significantly impacted Sr migration. The formation of bubbles and He-induced holes created pathways for Sr out-diffusion, thereby reducing Sr retention within the SiC structure. However, the He-induced cavities facilitated the trapping of Sr atoms.

These results highlight the potential challenges posed by the presence of He in TRISO fuel particles. These results have the potential to significantly influence the development of more durable and efficient TRISO fuel particles, thereby improving the performance and safety of nuclear reactors, particularly in next-generation designs. However, further comprehensive investigations are needed to validate these findings and assess their implications for fuel performance.

CRediT authorship contribution statement

T.T. Hlatshwayo: Writing – review & editing, Writing – original draft, Methodology, Investigation, Conceptualization. **T.F. Mokgadi:** Writing – original draft, Formal analysis. **S.S. Ntshangase:** Writing – review & editing, Resources. **Z.A.Y. Abdalla:** Writing – original draft, Investigation. **E.G. Njoroge:** Writing – review & editing, Writing – original draft. **T. Nguyen:** Formal analysis. **A. Sohatsky:** Formal analysis. **V.A. Skuratov:** Writing – original draft, Methodology.

Declaration of competing interest

The authors declare that they have no known competing financial interests or personal relationships that could have appeared to influence the work reported in this paper.

Acknowledgements

This study was financially supported by the National Research Foundation (NRF) of South Africa (grant numbers:2204072593,30308881411 and 23040388976) which is gratefully acknowledged. This work was also supported by the Ministry of Science and Higher Education of the Russian Federation-contract 075-15-2021-709, unique identifier of the project RF-2296.61321X0037.

Appendix A. Supplementary data

Supplementary data to this article can be found online at https://doi.org/10.1016/j.ceramint.2025.03.140.

References

[1] N.G. Van der Berg, J.B. Malherbe, A.J. Botha, E. Friedland, Thermal etching of SiC, Appl. Surf. Sci. 258 (15) (2012) 5561–5566, https://doi.org/10.1016/j.apsusc.2011.12.132.
[2] J.B. Malherbe, Diffusion of fission products and radiation damage in SiC, J. Phys. 46 (47) (2013) 473001, https://doi.org/10.1088/0022-3727/46/47/473001.
[3] Y. Katoh, L.L. Snead, I. Szlufarska, W.J. Weber, Radiation effects in SiC for nuclear structural applications, Curr. Opin. Solid State Mater. Sci. 16 (3) (2012) 143–152, https://doi.org/10.1016/j.cossms.2012.03.005.
[4] J.B. Malherbe, E. Friedland, N.G. Van Der Berg, Ion beam analysis of materials in the PBMR reactor, Nucl. Instrum. Methods Phys. Res. B. 266 (8) (2008) 1373–1377, https://doi.org/10.1016/j.nimb.2007.10.046.
[5] INTERNATIONAL ATOMIC ENERGY AGENCY, Fuel Performance and Fission Product Behaviour in Gas-Cooled Reactors, IAEA, Vienna, 1997. IAEA-TECDOC-978, http://www-pub.iaea.org/books/IAEABooks/5633/Fuel-Performance-and-Fission-ProductBehaviour-in-GasCooled-Reactors.
[6] M.R. Gilbert, S.L. Dudarev, D. Nguyen-Manh, S. Zheng, L.W. Packer, J.C. Sublet, Neutron-induced dpa, transmutations, gas production, and helium embrittlement of fusion materials, J. Nucl. Mater. 442 (1–3) (2013) S755–S760, https://doi.org/10.1016/j.jnucmat.2013.03.085.
[7] B.S. Li, Y.Y. Du, Z.G. Wang, Recrystallization of He-ion implanted 6H-SiC upon annealing, Nucl. Instrum. Methods Phys. Res. B. 345 (2015) 53–57, https://doi.org/10.1016/j.nimb.2014.12.049.
[8] N. Cherkashin, N. Daghbouj, G. Seine, A. Claverie, Impact of He and H relative depth distributions on the result of sequential He+ and H+ ion implantation and annealing in silicon, J. Appl. Phys. 123 (16) (2018) 161556, https://doi.org/10.1063/1.5012505.
[9] N. Daghbouj, B.S. Li, M. Callisti, H.S. Sen, J. Lin, X. Ou, M. Karlik, T. Polcar, The structural evolution of light-ion implanted 6H-SiC single crystal: comparison of the effect of helium and hydrogen, Acta Mater. 188 (2020) 609–622, https://doi.org/10.1016/j.actamat.2020.02.046.
[10] E. Oliviero, M.F. Beaufort, J.F. Barbot, A. Van Veen, A.V. Fedorov, Helium implantation defects in SiC: a thermal helium desorption spectrometry investigation, J. Appl. Phys. 93 (1) (2003) 231–238, https://doi.org/10.1063/1.1527974.
[11] R.W. Harrison, S. Ebert, J.A. Hinks, S.E. Donnelly, Damage microstructure evolution of helium ion irradiated SiC under fusion relevant temperatures, J. Eur. Ceramic Soc. 38 (11) (2018) 3718–3726, https://doi.org/10.1016/j.jeurceramsoc.2018.04.060.
[12] N. Daghbouj, N. Cherkashin, A. Claverie, A method to determine the pressure and densities of gas stored in blisters: application to H and He sequential ion implantation in silicon, Microelectron. Eng. 190 (2018) 54–56, https://doi.org/10.1016/j.mee.2018.01.006.
[13] B.S. Li, Z.G. Wang, H.P. Zhang, Study of surface blistering in GaN by hydrogen implantation at elevated temperatures, Thin Solid Films 590 (2015) 64–70, https://doi.org/10.1016/j.tsf.2015.07.039.
[14] F.I. Allen, P. Hosemann, M. Balooch, Key mechanistic features of swelling and blistering of helium-ion-irradiated tungsten, Scr. Mater. 178 (2020) 256–260, https://doi.org/10.1016/j.scriptamat.2019.11.039.
[15] H. Zang, W. Jiang, W. Liu, A. Devaraj, D.J. Edwards, C.H. Henager Jr., R.J. Kurtz, T. Li, C. He, D. Yun, Z. Wang, Vacancy effects on the formation of He and Kr cavities in 3C-SiC irradiated and annealed at elevated temperatures, Nucl. Instrum. Methods Phys. Res. B. 389 (2016) 40–47, https://doi.org/10.1016/j.nimb.2016.11.017.
[16] T.T. Hlatshwayo, C.E. Maepa, M. Msimanga, M. Mlambo, E.G. Njoroge, V. A. Skuratov, S.V. Motloung, J.B. Malherbe, Helium assisted migration of silver implanted into SiC, Vac 183 (2021) 109865, https://doi.org/10.1016/j.vacuum.2020.109865.
[17] B.S. Li, H.S. Sen, N. Daghbouj, A.T. AlMotasem, J. Lorinčík, M. Karlik, F.F. Ge, L. Zhang, Z. Sofer, I. Elantyev, M. Callisti, Thermal behavior of iron in 6H-SiC: influence of He-induced defects, Scr. Mater. 218 (2022) 114805, https://doi.org/10.1016/j.scriptamat.2022.114805.
[18] G. You, S. Wang, H. Zhang, W. Li, X. Guo, S. Ru, B. Li, Chemical disorder in 6H-SiC irradiated with both He and Fe ions followed by 1500° C annealing: electron energy-loss spectroscopy analysis, Crystals 12 (5) (2022) 687, https://doi.org/10.3390/cryst12050687.
[19] N. Daghbouj, A.T. AlMotasem, J. Vesely, B.S. Li, H.S. Sen, M. Karlik, J. Lorinčík, F. F. Ge, L. Zhang, V. Krsjak, O. Laguta, Microstructure evolution of iron precipitates in (Fe, He)-irradiated 6H-SiC: a combined TEM and multiscale modeling, J. Nucl. Mater. (2023) 154543, https://doi.org/10.1016/j.jnucmat.2023.154543.
[20] H.S. Sen, N. Daghbouj, B.S. Li, A.T. AlMotasem, F.F. Ge, L. Zhang, M. Callisti, T. Polcar, Interaction of Stacking Faults with point/extended defects in Fe-He irradiated 6H-SiC, Acta Mater. 256 (2023) 119129.
[21] T. Mokgadi, Z. Abdalla, H. Abdelbagi, M. Msimanga, C. Maepa, V. Skuratov, T. Hlatshwayo, Helium and strontium co-implantation into SiC at room temperature and isochronal annealing: structural evolution of SiC and migration behaviour of strontium, Mater. Chem. Phys. (2023) 126998, https://doi.org/10.1016/j.matchemphys.2022.126998.
[22] T.T. Hlatshwayo, T.F. Mokgadi, A. Sohatsky, Z.A.Y. Abdalla, V.A. Skuratov, E. G. Njoroge, M. Mlambo, The migration behaviour of strontium co-implanted with helium into SiC at room temperature and annealed at temperatures above 1000 °C, Vacuum 230 (2024) 113676.

[23] T.F. Mokgadi, Z.A.Y. Abdalla, M. Madhuku, E.G. Njoroge, M. Mlambo, P. Mdluli, A. Sohatsky, V.A. Skuratov, J.B. Malherbe, T.T. Hlatshwayo, The influence of helium-induced defects on the migration of strontium implanted into SiC above critical amorphization temperature, Front. Mater. (2023) 1192989, https://doi.org/10.3389/fmats.2023.1192989.
[24] G. Ntshobeni, Z.A.Y. Abdalla, T.F. Mokgadi, M. Mlambo, E.G. Njoroge, M. Msimanga, A. Sohatsky, V.A. Skuratov, T.T. Hlatshwayo, The effects of helium, strontium, and silver triple ions implanted into SiC, Heliyon (2023) 20877, https://doi.org/10.1016/j.heliyon.2023.e20877.
[25] S.Z. Mtsi, A. Sohatsky, Z.A.Y. Abdalla, E.G. Njoroge, V.A. Skuratov, S.V. Motloung, T.T. Hlatshwayo, Effects of helium (He) bubbles and annealing on the structural evolution and migration behavior of silver (Ag) implanted into polycrystalline SiC at 350° C, Vacuum 218 (2023) 112621, https://doi.org/10.1016/j.vacuum.2023.112621.
[26] E. Friedland, J.B. Malherbe, N.G. Van der Berg, T. Hlatshwayo, A.J. Botha, E. Wendler E., W. Wesh, Study of silver diffusion in silicon carbide, J. Nucl. Mater. 2009 (2009) 389, https://doi.org/10.1016/j.jnucmat.2009.02.022.
[27] J.F. Ziegler, M.D. Ziegler, J.P. Biersack, Srim – the stopping and range of ions in matter (2010), Nucl. Instrum. Methods Phys. Res. B 268 (2010) 1818–1823, https://doi.org/10.1016/j.nimb.2010.02.091.
[28] W. Wendler, A. Heft, W. Wesch, Ion-beam induced damage and annealing behaviour in SiC, Nucl. Instrum. Methods Phys. Res. B. 141 (1–4) (1998) 105–117, https://doi.org/10.1016/S0168-583X(98)00083-4.
[29] E. Friedland, N.G. van der Berg, J.B. Malherbe, E. Wendler, W. Wesch, Influence of radiation damage on strontium and iodine diffusion in silicon carbide, J. Nucl. Mater. 425 (1–3) (2012) 205–210, https://doi.org/10.1016/j.jnucmat.2011.10.032.
[30] T.T. Hlatshwayo, N. Mtshonisi, E.G. Njoroge, M. Mlambo, M. Msimanga, V. A. Skuratov, J.B. Malherbe, S.V. Motloung, Effects of Ag and Sr dual ions implanted into SiC, Nucl. Instrum. Methods Phys. Res. B. 472 (2020) 7–13, https://doi.org/10.1016/j.nimb.2020.03.035.
[31] G.J. Butterworth, Low activation structural materials for fusion, Fusion Eng. Des. 11 (1–2) (1989) 231–244, https://doi.org/10.1016/0920-3796(89)90021-5.
[32] K.A. Terrani, B.A. Pint, C.M. Parish, C.M. Silva, L.L. Snead, Y. Katoh, Silicon carbide oxidation in steam up to 2 MPa, J. Am. Ceram. Soc. 97 (8) (2014) 2331–2352, https://doi.org/10.1111/jace.13094.
[33] A. Barcz, M. Kozubal, R. Jakieła, J. Ratajczak, J. Dyczewski, K. Gołaszewska, T. Wojciechowski, G.K. Celler, Diffusion and impurity segregation in hydrogen-implanted silicon carbide, J. Appl. Phys. 115 (22) (2014) 223710, https://doi.org/10.1063/1.4882996.
[34] J. Grisolia, F. Cristiano, B. De Mauduit, G.B. Assayag, F. Letertre, B. Aspar, L. Di Cioccio, A. Claverie, Kinetic aspects of the growth of hydrogen induced platelets in SiC, J. Appl. Phys. 87 (12) (2000) 8415–8419, https://doi.org/10.1063/1.373556.
[35] C.H. Chen, Y. Zhang, Y. Wang, M.L. Crespillo, C.L. Fontana, J.T. Graham, G. Duscher, S.C. Shannon, W.J. Weber, Dose dependence of helium bubble formation in nano-engineered SiC at 700° C, J. Nucl. Mater. 472 (2016) 153–160, https://doi.org/10.1016/j.jnucmat.2016.01.029.
[36] J.A. Hinks, J.A. Van Den Berg, S.E. Donnelly, MIAMI: microscope and ion accelerator for materials investigations, J. Vac. Sci. Technol. A: Vac. Surf. Films 29 (2) (2011) 021003, https://doi.org/10.1116/1.3543707.
[37] B.S. Li, Z.G. Wang, C.H. Zhang, K.F. Wei, C.F. Yao, J.R. Sun, M.H. Cui, Y.F. Li, H. P. Zhu, Y.Y. Du, Y.B. Zhu, Evolution of strain and mechanical properties upon annealing in He-implanted 6H-SiC, J. Nucl. Mater. 455 (1–3) (2014) 116–121, https://doi.org/10.1016/j.jnucmat.2014.05.028.
[38] F. Linez, F. Garrido, H. Erramli, T. Sauvage, B. Courtois, P. Desgardin, M.F. Barthe, Experimental location of helium atoms in 6H–SiC crystal lattice after implantation and after annealing at 400° C, J. Nucl. Mater. 459 (2015) 62–69, https://doi.org/10.1016/j.jnucmat.2014.12.118.
[39] F. Linez, E. Gilabert, A. Debelle, P. Desgardin, M.F. Barthe, Helium interaction with vacancy-type defects created in silicon carbide single crystal, J. Nucl. Mater. 436 (1–3) (2013) 150–157, https://doi.org/10.1016/j.jnucmat.2013.01.288.
[40] C.H. Zhang, S.E. Donnelly, V.M. Vishnyakov, J.H. Evans, Dose dependence of formation of nanoscale cavities in helium-implanted 4H–SiC, J. Appl. Phys. 94 (9) (2003) 6017–6022, https://doi.org/10.1063/1.1611630.
[41] J. Sun, B.S. Li, Y.W. You, J. Hou, Y. Xu, C.S. Liu, Q.F. Fang, Z.G. Wang, The stability of vacancy clusters and their effect on helium behaviors in 3C-SiC, J. Nucl. Mater. 503 (2018) 271–278, https://doi.org/10.1016/j.jnucmat.2018.03.010.
[42] Zhiqiang Wang, Limin Zhang, Tamer AlMotasem Ahmed, Bingsheng Li, Tomas Polcar, Nabil Daghbouj, Exploring defect behavior in helium-irradiated single-crystal and nanocrystalline 3C-SiC at 800 °C: simulation techniques, Acta Mater. 279 (2024).
[43] Z.A.Y. Abdalla, M.Y.A. Ismail, E.G. Njoroge, T.T. Hlatshwayo, E. Wendler, J. B. Malherbe, Migration behaviour of selenium implanted into polycrystalline 3C–SiC, Vacuum 175 (2020) 109235, https://doi.org/10.1016/j.vacuum.2020.109235.
[44] W. Wesch, A. Heft, E. Wendler, T. Bachmann, E. Glaser, High temperature ion implantation of silicon carbide, Nucl. Instrum. Methods Phys. Res. B. 96 (1–2) (1995) 335–338, https://doi.org/10.1016/0168-583X(94)00513-3.
[45] J.B. Malherbe, N.G. Van Der Berg, A.J. Botha, E. Friedland, T.T. Hlatshwayo, R. J. Kuhudzai, E. Wendler, W. Wesch, P. Chakraborty, E.F. Da Silveira, SEM analysis of ion implanted SiC, Nucl. Instrum. Methods Phys. Res. B. 315 (2013) 136–141, https://doi.org/10.1016/j.nimb.2013.04.073.
[46] N. Daghbouj, J. Lin, H.S. Sen, M. Callisti, B. Li, M. Karlik, T. Polcar, Z. Shen, M. Zhou, T. You, X. Ou, Blister formation in He-H co-implanted InP: a comprehensive atomistic study, Appl. Surf. Sci. 552 (2021) 149426, https://doi.org/10.1016/j.apsusc.2021.149426.
[47] N. Daghbouj, B.S. Li, M. Karlik, A.J.A.S.S. Declemy, 6H-SiC blistering efficiency as a function of the hydrogen implantation fluence, Appl. Surf. Sci. 466 (2019) 141–150, https://doi.org/10.1016/j.apsusc.2018.10.005.
[48] W. Han, B. Li, Microstructural defects in He-irradiated polycrystalline α-SiC at 1000° C, J. Nucl. Mater. 504 (2018) 161–165, https://doi.org/10.1016/j.jnucmat.2018.03.038.
[49] B.S. Li, Y.Y. Du, Z.G. Wang, K.F. Wei, H.P. Zhang, C.F. Yao, H.L. Chang, J.R. Sun, M.H. Cui, Y.B. Sheng, L.L. Pang, Transmission electron microscopy investigations of bubble formation in He-implanted polycrystalline SiC, Vacuum 113 (2015) 75–83, https://doi.org/10.1016/j.vacuum.2014.12.017.
[50] M. Liu, X. Yang, Y. Gao, R. Liu, H. Huang, X. Zhou, T.K. Sham, Investigation of the damage behavior in CVD SiC irradiated with 70 keV He ions by NEXAFS, Raman and TEM, J. Eur. Ceram. Soc. 37 (4) (2017) 1253–1259, https://doi.org/10.1016/j.jeurceramsoc.2016.11.046.
[51] E. Oliviero, M.L. David, M.F. Beaufort, J. Nomgaudyte, L. Pranevicius, A.B.J. F. Declemy, J.F. Barbot, Formation of bubbles by high dose He implantation in 4H–SiC, J. Appl. Phys. 91 (3) (2002) 1179–1186, https://doi.org/10.1063/1.1429760.